

Slowdown of the Walker circulation driven by tropical Indo–Pacific warming

Hiroki Tokinaga¹, Shang–Ping Xie^{1,2}, Clara Deser³, Yu Kosaka⁴ & Yuko M. Okumura⁵

Global mean sea surface temperature (SST) has risen steadily over the past century^{1,2}, but the overall pattern contains extensive and often uncertain spatial variations, with potentially important effects on regional precipitation^{3,4}. Observations suggest a slowdown of the zonal atmospheric overturning circulation above the tropical Pacific Ocean (the Walker circulation) over the twentieth century^{1,5}. Although this change has been attributed to a muted hydrological cycle forced by global warming^{5,6}, the effect of SST warming patterns has not been explored and quantified^{1,7,8}. Here we perform experiments using an atmospheric model, and find that SST warming patterns are the main cause of the weakened Walker circulation over the past six decades (1950–2009). The SST trend reconstructed from bucket-sampled SST and night-time marine surface air temperature features a reduced zonal gradient in the tropical Indo-Pacific Ocean, a change consistent with subsurface temperature observations⁸. Model experiments with this trend pattern robustly simulate the observed changes, including the Walker circulation slowdown and the eastward shift of atmospheric convection from the Indonesian maritime continent to the central tropical Pacific. Our results cannot establish whether the observed changes are due to natural variability or anthropogenic global warming, but they do show that the observed slowdown in the Walker circulation is presumably driven by oceanic rather than atmospheric processes.

The Walker circulation is a defining feature of tropical climate. On seasonal-to-interannual timescales, it is closely tied to the east–west SST gradient along the Equator, as is the El Niño–Southern Oscillation (ENSO). Long-term changes in the Walker circulation have recently been the subject of intense debate^{1,5–12}. Most climate models in the Coupled Model Intercomparison Project phase 3 (CMIP3) predict a slowdown of the Walker circulation under global warming^{5–7,9,13}, consistent with sea level pressure (SLP) measurements during the twentieth century^{1,5,8}. The Walker circulation weakening relaxes prevailing easterly trade winds over the equatorial Pacific^{5,8} and suppresses the upwelling of nutrient-rich cold water⁷, affecting fishery stocks in the region. Despite these important climatic and biogeochemical influences, the mechanism for the observed long-term change in the Walker circulation has not been rigorously investigated.

One major hypothesis attributes the Walker circulation slowdown to a decrease in convective mass flux under global warming that balances a slower increase in global mean precipitation than can be expected from the increase in atmospheric water vapour⁶. This muted hydrological cycle mechanism relies only on a globally uniform increase in SST³. Overlooked, however, is an alternative hypothesis that points to changes in zonal SST gradient across the tropical oceans^{1,11,14}. This mechanism is dominant for ENSO, but the effort to test its role in the long-term weakening of the Walker circulation has been hampered by uncertainty in observed SST warming patterns^{1,7,8}. For 1950–2009, the zonal SST gradient across the Indo-Pacific has intensified in the HadISST1 (Hadley Centre sea ice and SST

version 1; ref. 15) data set but shows little change in the ERSST3b (extended reconstructed SST version 3b; ref. 16) data set (Fig. 1). This disagreement is due to the change in SST measurement technique and different analysis methods⁷.

We reconstruct the SST trend pattern for the period 1950–2009 (Fig. 1a), for which various data sets are available with improved quality. To reduce biases caused by changes in SST measurement technique, we construct an SST data set using only bucket measurements from the International Comprehensive Ocean–Atmosphere Data Set¹⁷ (COADS). The resulting trend pattern exhibits a reduced zonal gradient between the eastern Pacific and the western Pacific/southeastern Indian Ocean (Supplementary Fig. 1a), in contrast to HadISST1 and ERSST3b results (Fig. 1b, c). We also examine night-time marine surface air temperature (NMAT), a meteorological parameter that is highly correlated with SST (Supplementary Fig. 2) but free of the biases introduced by changes in SST measurement technique. The NMAT trend pattern bears a striking resemblance to that of bucket SST (Supplementary Fig. 1b, c). This motivates us to estimate trends in merged surface temperature (MST) of the bucket SST and NMAT (see Methods). The MST trend features a reduced zonal gradient in the tropical Indo-Pacific (Fig. 1a, d), physically consistent with a flattened ocean thermocline observed by expendable bathythermographs⁸.

To investigate the SST gradient effect, we use four atmospheric general circulation models (AGCMs; see Methods) and construct a multi-model ensemble for an unbiased estimate of the atmospheric response. Each AGCM is forced with four different tropical SST trend patterns: a spatially uniform SST increase (SUSI; $\sim 0.5^\circ\text{C}$ for 60 yr from 1950 to 2009) and those estimated from MST, HadISST1 and ERSST3b. In all the experiments including SUSI, the greenhouse-gas increase from the 1950s to the 2000s is imposed. The AGCM response to SUSI is not an accurate proxy for anthropogenic change, but serves as a useful reference to evaluate the SST pattern effect. To validate the model experiments, we use a wide variety of data sets, all of which have successfully captured regional patterns of tropical climate change^{1,8} (Methods). We also use 71 ensemble members of the ‘climate of the twentieth century’ experiments (20C3M) from 24 CMIP3 models and three atmospheric reanalyses for comparison: the US National Centers for Environmental Prediction (NCEP)–National Center for Atmospheric Research (NCAR) reanalysis¹⁸, the European Centre for Medium-Range Weather Forecasting 40-year reanalysis (ERA-40; ref. 19), and the Twentieth Century Reanalysis version 2 (20CrV2; ref. 20).

Over the past six decades, a weakening trend in the Walker circulation is apparent in SLP change^{1,8,9} (Fig. 1a and Supplementary Fig. 3a), increasing over the maritime continent and decreasing east of the Philippines and over the central to eastern tropical Pacific. The MST-forced experiments reproduce these SLP change patterns quite well, with a slight eastward displacement of negative values over the eastern Pacific (Fig. 1d). In contrast, the HadISST1-forced experiments strengthen the Walker circulation¹² (Fig. 1b), while the ERSST3b experiments show no significant change (Fig. 1c). The SUSI-forced

¹International Pacific Research Center, Department of Meteorology, SOEST, University of Hawaii at Manoa, 1680 East West Road, Honolulu, Hawaii 96822, USA. ²Physical Oceanography Laboratory, Ocean University of China, Qingdao 266003, China. ³National Center for Atmospheric Research, PO Box 3000, Boulder, Colorado 80307, USA. ⁴International Pacific Research Center, SOEST, University of Hawaii at Manoa, 1680 East West Road, Honolulu, Hawaii 96822, USA. ⁵Institute for Geophysics, The University of Texas at Austin, 10100 Burnet Road, Austin, Texas 78758, USA.

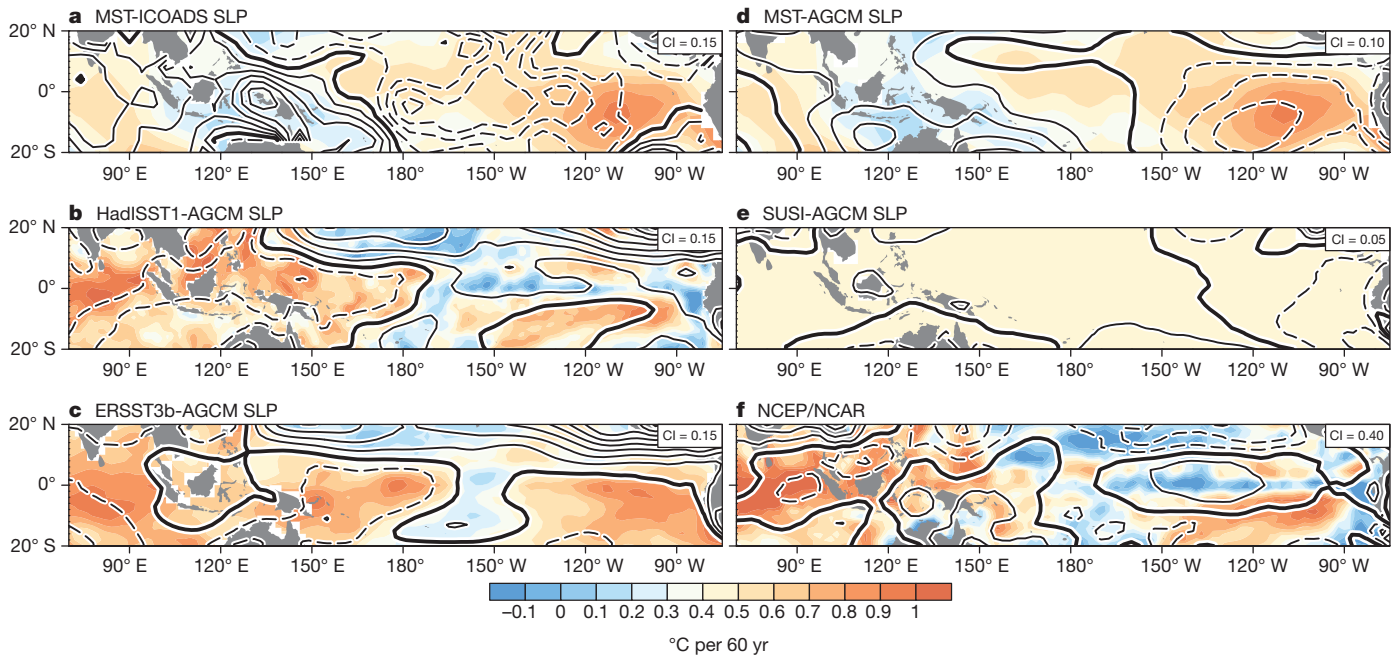


Figure 1 | Observed and simulated patterns of SLP and SST changes for 1950–2009. Changes in SLP (hPa per 60 yr; contours) and SST ($^{\circ}\text{C}$ per 60 yr; shading) from: **a**, ICOADS and MST; **b**, HadISST1-forced experiment; **c**, ERSST3b-forced experiment; **d**, MST-forced experiment; **e**, SUSI-forced

experiment; and **f**, NCEP-NCAR reanalysis. The contour interval (CI) for SLP change is indicated at the top-right corner of each panel. Positive (negative) contours are solid (dashed) lines, and zero contours are thickened. The basin averages (40°E – 70°W , 20°S – 20°N) of SLP change are removed.

experiments simulate a slight weakening of the Walker circulation (Fig. 1e) but its magnitude is much weaker than that of observations⁹ and MST-forced experiments. These AGCM experiments suggest that SST trend patterns are key to the Walker circulation change.

Both the NCEP-NCAR (Fig. 1f) and ERA-40 (Supplementary Fig. 3b) reanalyses show an intensification of the Walker circulation with SLP increasing over the central equatorial Pacific and decreasing over the maritime continent. The SST data sets used in these reanalyses exhibit an intensified zonal gradient similar to that in HadISST1, suggesting a strong impact of SST forcing even in the NCEP-NCAR and ERA-40 reanalyses. The 20CRv2 reanalysis exhibits no significant change in SLP gradient despite the assimilation of SLP observations (Supplementary Fig. 3c). HadISST1 is used as a surface forcing in 20CRv2, which we speculate acts to oppose the observed reduction in the Walker circulation.

Changes in atmospheric convection are a clue to the Walker circulation slowdown. Observations indicate an eastward shift of precipitation/cloudiness from the maritime continent to the central tropical Pacific, accompanied by consistent changes in surface wind convergence (Fig. 2a, b). The MST-forced experiments simulate these patterns of cloud, precipitation and surface wind changes quite well, albeit at reduced magnitudes (Fig. 2c, d). The simulated convection changes closely follow spatial patterns of SST warming, consistent with the “warmer-get-wetter” idea, with support from model projections³ and satellite observations for the past three decades²¹. In contrast, the SUSI experiments simulate a precipitation/cloudiness increase over the maritime continent (Fig. 2e, f), in disagreement with observations. Within the framework of our AGCM experiments, SST warming patterns, rather than the hydrological cycle response to uniform warming, is the main driver for the Walker circulation slowdown and atmospheric convection changes over the past six decades.

The close linkage between SST and the Walker circulation is readily illustrated in a scatter plot of changes in zonal SST and SLP gradients (denoted ΔSST and ΔSLP , respectively), defined as the zonal difference on the Equator between the eastern Pacific (150° – 90°W , 5°S – 5°N) and western Pacific/eastern Indian Ocean (90° – 150°E , 5°S – 5°N) (Fig. 3). Changes in ΔSST and ΔSLP are linearly correlated among

AGCM experiments and reanalyses ($r \approx -0.97$, significant at $P < 0.01$), with a strong dependence on SST data sets. MST-forced (HadISST1-forced) AGCMs robustly simulate a weakening (strengthening) of ΔSLP in response to the ΔSST weakening (strengthening), whereas ERSST3b-forced AGCMs show little change in ΔSLP . SUSI-forced AGCMs tend to weaken ΔSLP , but this is not robust among models and the amplitude is small. Overall, MST-forced AGCMs simulate the observed ΔSLP change more realistically than other SST data sets. In addition, ΔSLP and ΔSST are highly correlated among the 71 simulations in the CMIP3 20C3M ensemble ($r \approx -0.83$, significant at $P < 0.01$), although the ΔSLP reduction is smaller than in observations⁹.

We estimate uncertainty in SST trends arising from observational biases based on 100 realizations of SST data in the third version of the Hadley Centre gridded SST data set (HadSST3; refs 2, 22). There are large variations in ΔSST among different realizations (Figs 3 and 4a). We apply empirical orthogonal function (EOF) analysis to the 1950–2006 trend patterns over the tropical Indo-Pacific (30°E – 60°W , 32.5°S – 32.5°N) from the 100 realizations. The leading EOF reveals large uncertainty in warming magnitude over the equatorial Indo-western Pacific, accounting for 83.6% of the total variance among the 100 SST realizations (Supplementary Fig. 4a). The correlation between the principal component of the leading EOF and the ΔSST trend is -0.75 (significant at $P < 0.01$), indicating that the ΔSST trend is strongly affected by uncertainty in the magnitude of SST warming over the equatorial Indo-western Pacific (Fig. 4a). Nevertheless, all the HadSST3 realizations show a reduction in ΔSST . AGCM experiments forced by a subset of HadSST3 realizations, including the two extremes (no. 12 and no. 34) and median, all simulate the Walker circulation slowdown (Fig. 4b–e), with SLP increasing (decreasing) over the maritime continent (tropical Pacific). The magnitude of circulation change is proportional to that of ΔSST (green triangles in Fig. 3). These HadSST3 experiments provide strong support for our results from observations and MST-forced AGCMs.

Our AGCM results show that the observed Walker circulation slowdown is due to the weakened zonal SST gradient across the equatorial

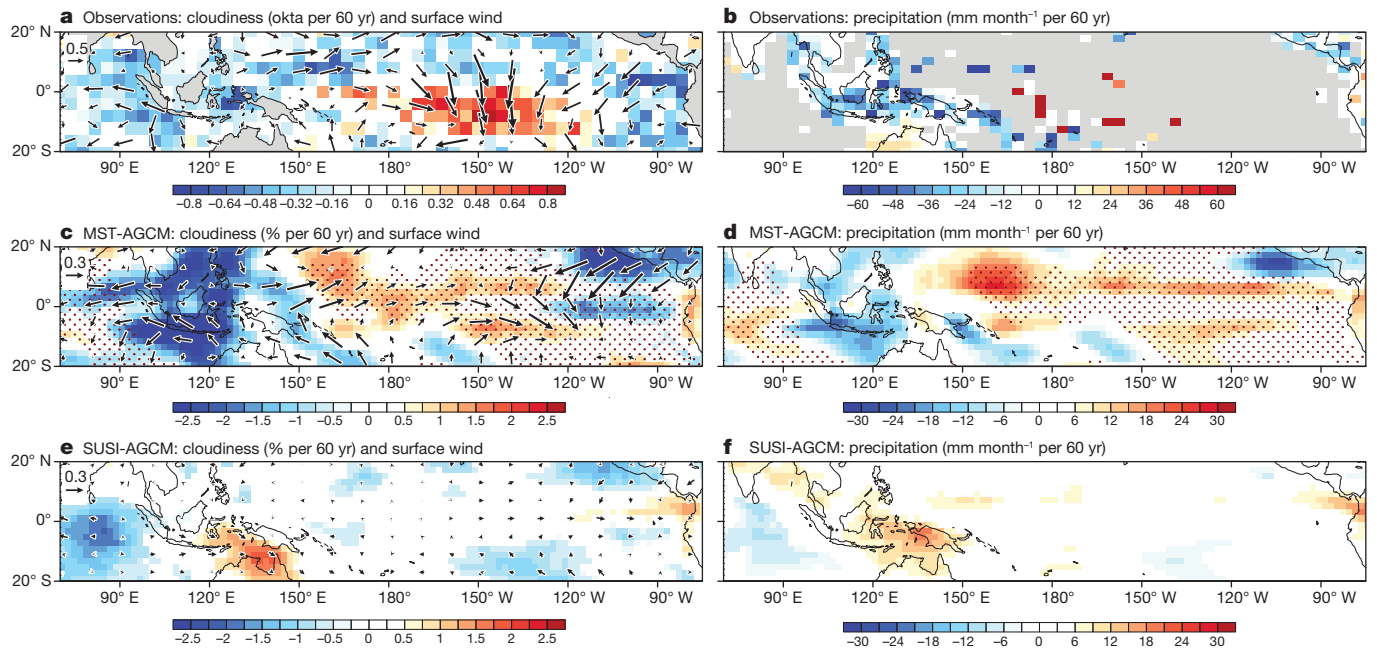


Figure 2 | Observed and simulated changes in cloudiness, surface wind and precipitation for 1950–2009. Changes in cloudiness (okta per 60 yr for observation, % per 60 yr for AGCM; shading in left panels), surface wind (m s^{-1} per 60 yr; vectors in left panels), and precipitation (mm month^{-1} per 60 yr; shading in right panels) from: **a, b**, observations (ICOADS, WASWind and

rain-gauges); **c, d**, MST-forced experiment; and **e, f**, SUSI-forced experiment. Only significant changes exceeding the 95% confidence level are shaded in colour. Stippling in **c, d**, indicates regions of the MST warming trend above the tropical mean.

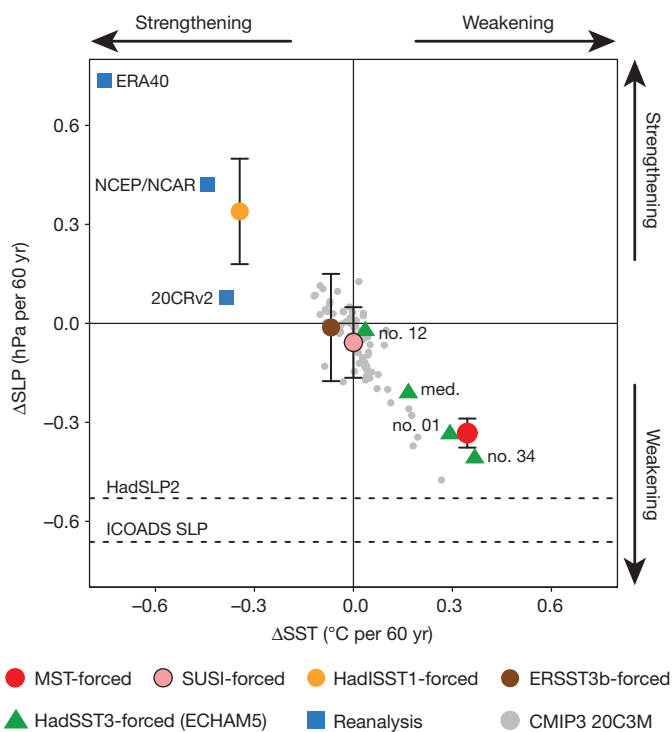


Figure 3 | Scatter diagram of Δ SST and Δ SLP changes in AGCM and CMIP3 model simulations and reanalysis data sets. Confidence intervals (error bars) for AGCM experiments are computed from the standard deviation of four ensemble members, at the two-sided $P = 0.01$ level. The twentieth-century trends are estimated from each ensemble member of the CMIP3 20C3M experiment, and scaled to 60-yr trends. Dashed lines indicate Δ SLP changes calculated from ICOADS and HadSLP2. A correlation coefficient between Δ SLP and Δ SST for AGCM experiments and reanalyses (CMIP3) is -0.97 (-0.83), significant at $P < 0.01$. See key at bottom for meaning of symbols.

Indo-Pacific, rather than to the muted hydrological cycle under uniform warming^{5,6}. This SST pattern mechanism itself is not new^{1,11,14,23} but its dominance in tropical climate change over the past six decades is surprising, given the prevailing assumption that the Walker circulation slowdown occurs without the zonal SST gradient change. Conversely, the reduced zonal SST gradient is the response to the weakened easterly trades⁸. The circular results suggest a positive feedback between the Walker circulation and SST gradient. In light of modest changes in the 20C3M simulations (Fig. 3), the observed changes discussed here probably include the influence of natural variability superimposed on externally forced response^{9,24}. The majority of CMIP phase 5 (CMIP5) models project a weakened SST gradient across the equatorial Indo-Pacific in response to increased greenhouse-gas forcing, but its magnitude is not significant in the twentieth century (Supplementary Fig. 5). On the other hand, the increased aerosols due to economic development and biomass burning may also have contributed to the reduced SST warming over the Indo-western Pacific region²⁵. An open question still remains: to what degree does anthropogenic forcing contribute to the observed changes? A conclusive attribution will have to wait for longer observations and the growth of the forced response.

Research into future climate change relies heavily on numerical models, but model skill in simulating long-term changes is largely untested. Validating climate models against observed change is critical in building confidence in their future projections. The slowdown of the Walker circulation is a robust change observed for the past century and serves a useful testbed for model evaluation. Our results show that AGCMs are successful in reproducing the Walker circulation slowdown, provided that the correct pattern of SST warming is prescribed. Taken together, our SST analysis and AGCM experiments indicate a weakening of zonal SST gradient across the equatorial Indo-Pacific over the past six decades. Our study highlights uncertainties in the tropical Indo-Pacific warming pattern and their effect on the Walker circulation change. The effect of SST warming uncertainty may extend remotely to densely populated regions such as East Asia through the atmospheric bridge²⁶ (Supplementary Fig. 4b). Our analysis suggests

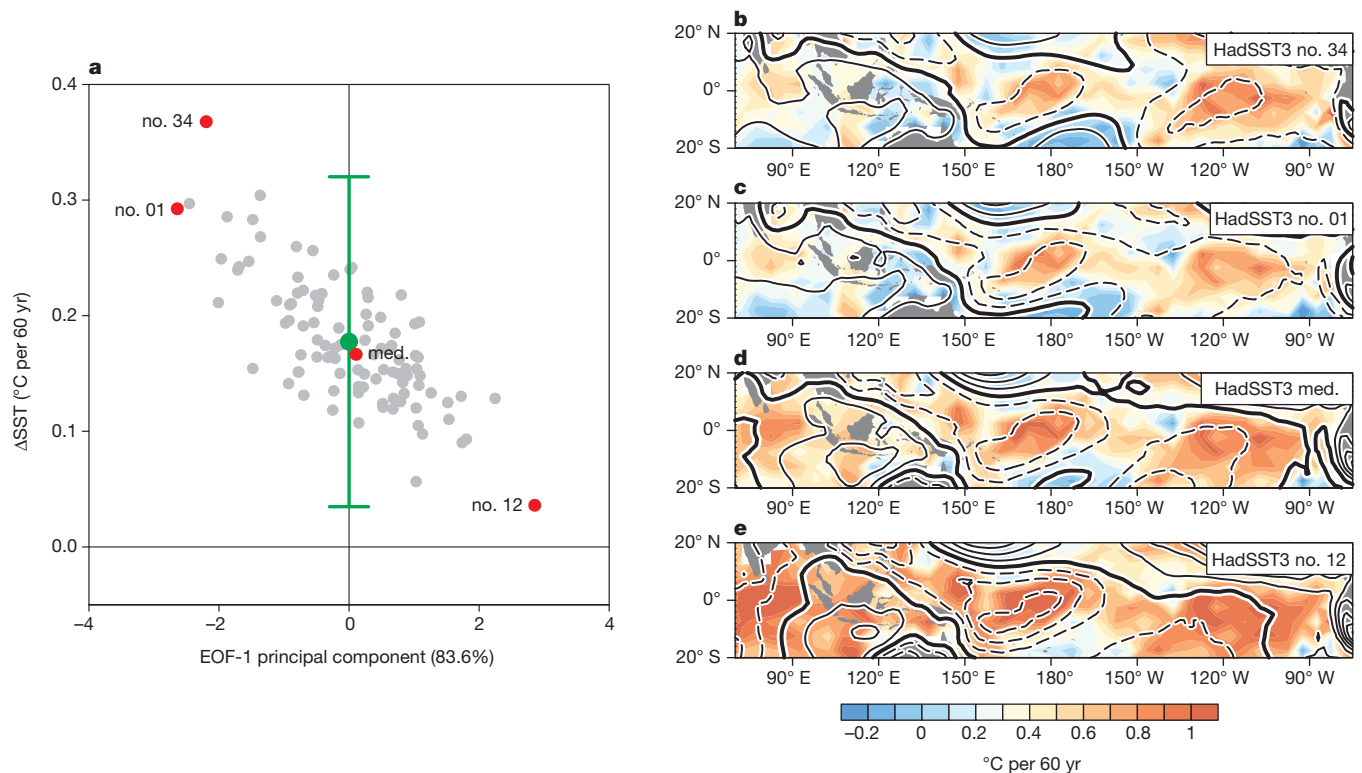


Figure 4 | Uncertainty in HadSST3 trends. **a**, Scatter diagram of Δ SST and the principal component of the leading EOF for the tropical Indo-Pacific SST trend patterns. The median and extreme realizations no. 01, no. 12, no. 34 of HadSST3 are indicated in red circles. Green circle indicates the ensemble mean of the HadSST3 realizations with the confidence interval at the

that atmospheric reanalyses are also subject to errors of SST warming pattern. Their judicious use is advised in studying long-term changes. Reducing biases and uncertainty in regional patterns of SST warming is a key step for improving the reanalyses and interpretation of long-term climate change.

METHODS SUMMARY

The MST trends were calculated for 1950–2009 as an unweighted average of the bucket SST and NMAT trends from ICOADS release 2.5 (ref. 17) and the Met Office Historical Marine Air Temperature 43N (MOHMAT; ref. 15). We performed a set of two AGCM experiments, in which the 30-yr-scaled MST trend pattern was either added to or subtracted from the HadISST1 climatology over the tropics only (20° S– 20° N). These two experiments were also forced with greenhouse-gas concentrations averaged in the 2000s and 1950s, respectively. By taking the difference between the two experiments, we extracted atmospheric changes over the past 60 yr. To investigate the effect of SST warming patterns, the same sets of AGCM experiments were forced by HadISST1, ERSST3b and HadSST3 trend patterns and SUSI ($\sim 0.5^{\circ}$ C increase per 60 yr). To obtain an unbiased estimate of the atmospheric response, we used four AGCMs: the US National Oceanic and Atmospheric Administration (NOAA) Geophysical Fluid Dynamics Laboratory (GFDL) AM2.1 (ref. 27), the Max Planck Institute (MPI) ECHAM5 (ref. 28), the NCAR Community Atmospheric Model (CAM) version 3 (ref. 29) and 4 (ref. 30). The AM2.1 (CAM4) uses a finite-volume grid of $2.5^{\circ} \times 2^{\circ}$ ($2.5^{\circ} \times 1.9^{\circ}$) longitude–latitude and 24 (26) vertical levels, and the ECHAM5 (CAM3) uses a T42 grid and 19 (26) vertical levels. For each experiment the models were integrated for 41 yr with the first year of integration discarded as a spin-up. Further details of observational data sets, AGCM experiments and analysis methods are discussed in Methods.

Full Methods and any associated references are available in the online version of the paper.

Received 21 April; accepted 11 September 2012.

- Deser, C., Phillips, A. S. & Alexander, M. A. Twentieth century tropical sea surface temperature trends revisited. *Geophys. Res. Lett.* **37**, L10701, <http://dx.doi.org/10.1029/2010GL043321> (2010).

two-sided $P = 0.01$ level (green error bar). **b–e**, SST (shading) and SLP (contour interval 0.15 hPa per 60 yr) changes from ECHAM5 experiments forced with HadSST3 realizations no. 34 (**b**), no. 01 (**c**), median (**d**) and no. 12 (**e**). Positive (negative) contours are solid (dashed) lines, and zero contours are thickened.

- Kennedy, J. J., Rayner, N. A., Smith, R. O., Parker, D. E. & Saunby, M. Reassessing biases and other uncertainties in sea surface temperature observations measured in situ since 1850: 2. Biases and homogenization. *J. Geophys. Res.* **116**, D14104, <http://dx.doi.org/10.1029/2010JD015220> (2011).
- Xie, S.-P. *et al.* Global warming pattern formation: sea surface temperature and rainfall. *J. Clim.* **23**, 966–986 (2010).
- Shin, S. I. & Sardeshmukh, P. D. Critical influence of the pattern of tropical ocean warming on remote climate trends. *Clim. Dyn.* **36**, 1577–1591 (2011).
- Vecchi, G. A. *et al.* Weakening of tropical Pacific atmospheric circulation due to anthropogenic forcing. *Nature* **441**, 73–76 (2006).
- Held, I. M. & Soden, B. J. Robust responses of the hydrological cycle to global warming. *J. Clim.* **19**, 5686–5699 (2006).
- Vecchi, G. A. & Soden, B. J. Global warming and the weakening of the tropical circulation. *J. Clim.* **20**, 4316–4340 (2007).
- Tokinaga, H. *et al.* Regional patterns of tropical Indo-Pacific climate change: evidence of the Walker circulation weakening. *J. Clim.* **25**, 1689–1710 (2012).
- Power, S. B. & Kociuba, G. What caused the observed twentieth-century weakening of the Walker circulation? *J. Clim.* **24**, 6501–6514 (2011).
- DiNezio, P., Clement, A. & Vecchi, G. A. Reconciling differing views of tropical Pacific climate change. *Eos* **91**, 141–142 (2010).
- Clement, A., DiNezio, P. & Deser, C. Rethinking the ocean's role in the Southern Oscillation. *J. Clim.* **24**, 4056–4072 (2011).
- Meng, Q. *et al.* Twentieth century Walker circulation change: data analysis and model experiments. *Clim. Dyn.* **38**, 1757–1773 (2012).
- Meehl, G. A. *et al.* in *Climate Change 2007: The Physical Science Basis* (eds Solomon, S. *et al.*) 747–845 (Cambridge Univ. Press, 2007).
- Bunge, L. & Clarke, A. J. A verified estimation of the El Niño index Niño-3.4 since 1877. *J. Clim.* **22**, 3979–3992 (2009).
- Rayner, N. A. *et al.* Global analyses of sea surface temperature, sea ice, and night marine air temperature since the late nineteenth century. *J. Geophys. Res.* **108**, 4407, <http://dx.doi.org/10.1029/2002JD002670> (2003).
- Smith, T. M., Reynolds, R. W., Peterson, T. C. & Lawrimore, J. Improvements to NOAA's historical merged land-ocean surface temperature analysis (1880–2006). *J. Clim.* **21**, 2283–2296 (2008).
- Woodruff, S. D. *et al.* ICOADS Release 2.5: extensions and enhancements to the surface marine meteorological archive. *Int. J. Climatol.* **31**, 951–967 (2011).
- Kalnay, E. *et al.* The NCEP/NCAR 40-year reanalysis project. *Bull. Am. Meteorol. Soc.* **77**, 437–471 (1996).
- Uppala, S. M. *et al.* The ERA-40 re-analysis. *Q. J. R. Meteorol. Soc.* **131**, 2961–3012 (2005).
- Compo, G. P. *et al.* The twentieth century reanalysis project. *Q. J. R. Meteorol. Soc.* **137**, 1–28 (2011).

21. Johnson, N. C. & Xie, S.-P. Changes in the sea surface temperature threshold for tropical convection. *Nature Geosci.* **3**, 842–845 (2010).
22. Kennedy, J. J., Rayner, N. A., Smith, R. O., Parker, D. E. & Saunby, M. Reassessing biases and other uncertainties in sea surface temperature observations measured in situ since 1850: 1. Measurement and sampling uncertainties. *J. Geophys. Res.* **116**, D14103, <http://dx.doi.org/10.1029/2010JD015218> (2011).
23. Deser, C. & Phillips, A. S. Simulation of the 1976/77 climate transition over the North Pacific: sensitivity to tropical forcing. *J. Clim.* **19**, 6170–6180 (2006).
24. Meehl, G. A., Hu, A. X. & Santer, B. D. The mid-1970s climate shift in the Pacific and the relative roles of forced versus inherent decadal variability. *J. Clim.* **22**, 780–792 (2009).
25. Ramanathan, V. *et al.* Atmospheric brown clouds: impacts on South Asian climate and hydrological cycle. *Proc. Natl Acad. Sci. USA* **102**, 5326–5333 (2005).
26. Xie, S.-P. *et al.* Decadal shift in El Niño influences on Indo-western Pacific and East Asian climate in the 1970s. *J. Clim.* **23**, 3352–3368 (2010).
27. The GFDL Global Atmospheric Model Development Team. The new GFDL global atmosphere and land model AM2–LM2: evaluation with prescribed SST simulations. *J. Clim.* **17**, 4641–4673 (2004).
28. Roeckner, E. *et al.* *The Atmospheric General Circulation Model ECHAM5. Part I: Model Description* (MPI report 349, Max Planck Institute, 2003); available at http://www.mpimet.mpg.de/fileadmin/publikationen/Reports/max_scirep_349.pdf (2003).
29. Collins, W. D. *et al.* The formulation and atmospheric simulation of the Community Atmosphere Model version 3 (CAM3). *J. Clim.* **19**, 2144–2161 (2006).
30. Neale, R. B. *et al.* The mean climate of the Community Atmosphere Model (CAM4) in forced SST and fully coupled experiments. *J. Clim.*. (submitted).

Supplementary Information is available in the online version of the paper.

Acknowledgements We thank A. Timmermann for discussions, and X. T. Zheng and J. Ma for data processing. The work was supported by JAMSTEC, the National Basic Research Program of China (2012CB955600), NASA, NSF and NOAA. NCAR is sponsored by NSF.

Author Contributions H.T., Y.K. and Y.M.O. designed and performed model experiments. S.-P.X. and C.D. supervised the work. H.T. analysed observations and model simulations. H.T., S.-P.X., C.D. and Y.M.O. wrote the manuscript, with feedback from all authors.

Author Information Reprints and permissions information is available at www.nature.com/reprints. The authors declare no competing financial interests. Readers are welcome to comment on the online version of the paper. Correspondence and requests for materials should be addressed to H.T. (tokenaga@hawaii.edu) and S.-P.X. (xie@hawaii.edu).

METHODS

SLP, SST and NMAT. For SLP, we used the ICOADS release 2.5 (ref. 17) and the Hadley Centre's mean SLP data set version 2 (HadSLP2; ref. 31). For SST, we used HadISST1 (ref. 15), ERSST3b (ref. 16), HadSST3 (refs 2, 22) and bucket-sampled SSTs from ICOADS. For surface air temperature, we analysed only night-time data because daytime observations are strongly biased by heating effects over ship decks. For NMAT, ICOADS and the Met Office Historical Marine Air Temperature (MOHMAT) 43N (ref. 15) were used. All ICOADS data have been trimmed using the climatological 4.5 standard-deviation limit that identifies potential outliers and then gridded on a 4° grid with an unweighted box average⁸. Missing data in ICOADS were filled with linear interpolation across 'no data' grids not exceeding 5 points in longitude and 3 points in latitude. This interpolation was applied twice to obtain basin-scale characteristics. For the MST trend patterns, we first calculated trends in bucket SST and NMAT separately, and then constructed an unweighted average of their trend patterns. To improve the readability, the MST trend patterns were spatially smoothed with a 5 × 5 point Gaussian filter. ICOADS (<http://rda.ucar.edu/datasets/ds540.0/>), HadSLP2 (<http://www.metoffice.gov.uk/hadobs/hadslp2/>), HadISST1 (<http://www.metoffice.gov.uk/hadobs/hadisst1/>), ERSST3b (<http://www.ncdc.noaa.gov/ersst/>), HadSST3 (<http://www.metoffice.gov.uk/hadobs/hadst3/>), MOHMAT43N (<http://www.metoffice.gov.uk/hadobs/mohmat/>) are all available online.

Surface wind. The Wave- and Anemometer-based Sea-surface Wind (WASWind) data set³² (<http://iprc.soest.hawaii.edu/users/tokinaga/waswind.html>) was used. This data set substantially reduces spurious upward trends in the ICOADS raw winds by applying bias corrections with a stability-dependent height correction for measured winds and using wind-wave height. The obtained trend patterns are in good agreement with SLP measurements since the 1950s and satellite measurements for recent decades, illustrating the utility for climate change studies.

Precipitation and cloudiness. We used four rain-gauge based monthly mean gridded products available at NOAA³³ (<http://www.esrl.noaa.gov/psd/data/gridded/data.precl.html>), the Global Precipitation Climatology Centre³⁴ (ftp://ftp.dwd.de/pub/data/gpcc/html/fulldata_v6_doi_download.html), the University of Delaware³⁵ (http://climate.geog.udel.edu/~climate/html_pages/Global2_Ts_2009/Global_p_ts_2009.html), and the University of East Anglia Climate Research Unit³⁶ (<http://www.cru.uea.ac.uk/cru/data/precip/>). All data were regridded onto a 3.75° × 2.5° longitude–latitude grid, and precipitation trends were calculated for 1950–2007 from an unweighted average of the four products. Marine cloudiness trends were calculated for 1950–2009 based on ICOADS. To eliminate the bias in ship-observed marine cloudiness, we removed the tropical (30° N–30° S) mean trend from each oceanic grid box¹.

Estimate of observed trends. All trends were calculated using only well-sampled grid boxes that contain monthly means for more than 75% of the total months. To suppress interannual variability for each month, all yearly data were smoothed with a five-point binominal temporal filter before the trend analysis. We estimated long-term trends and their statistical significance with the Sen median slope³⁷ and the Mann-Kendall³⁸ test, respectively, non-parametric methods less affected by outliers. The analysis period is basically from 1950 to 2009, but some data sets are not available for the entire period. In such cases, we scaled the trends to the 60-yr changes. Annual mean trends were presented in all figures.

AGCM experiments. We used the NOAA GFDL AM2.1 (ref. 27), the MPI ECHAM5 (ref. 28), the NCAR CAM3 (ref. 29) and CAM4 (ref. 30). The AM2.1

(CAM4) uses the finite-volume grid of 2.5° × 2° (2.5° × 1.9°) longitude–latitude and 24 (26) vertical levels, and the ECHAM5 (CAM3) uses a T42 grid and 19 (26) vertical levels. For each model and SST data set, we performed a set of two experiments, in which the 30-yr-scaled SST trend pattern was either added to or subtracted from the SST climatology over the tropics only (20° S–20° N). Two SST forcing fields were derived as follows:

$$\text{SST}_{\text{warm}} = \overline{\text{SST}} + 30 \text{SST}'$$

$$\text{SST}_{\text{cold}} = \overline{\text{SST}} - 30 \text{SST}'$$

where $\overline{\text{SST}}$ is the monthly SST climatology obtained from HadISST1, and SST' is the monthly mean SST trends per year estimated from each SST data set. Both $\overline{\text{SST}}$ and SST' were calculated for 1950–2009. For the SUSI experiment, we used a tropical mean SST trend of 0.0083 °C increase per year (~0.5 °C per 60 yr) based on the HadSST3 estimate. All SST forcing is yearly cycling data so that does not include interannual variability. The SST_{warm} and SST_{cold} experiments were also forced with greenhouse-gas concentrations (CO₂, CH₄, N₂O, CFC11, CFC12 and O₃) averaged in the 2000s and 1950s, respectively. By taking the difference between the two experiments, we extracted atmospheric changes over the past 60 yr. For each experiment the models were integrated for 41 yr with the first year of integration discarded as a spin-up. We used only ECHAM5 for HadSST3-forced experiments. The statistical significance for the difference between SST_{warm} and SST_{cold} experiments was estimated with the two-sided Student's *t*-test.

Other data sets. We used three atmospheric reanalysis products: the NCEP-NCAR reanalysis¹⁸ for 1950–2009 (<http://rda.ucar.edu/pub/reanalysis/index.html>), the ERA-40 reanalysis¹⁹ for 1958–2001 (<http://www.ecmwf.int/products/data/archive/descriptions/e4/index.html>), and 20CRv2 (ref. 20) for 1950–2008 (http://www.esrl.noaa.gov/psd/data/gridded/data.20thC_ReanV2.html). We also used the CMIP3 'Climate of the twentieth century experiments (20C3M)' (24 models) for 1900–1999, the CMIP5 historical run (22 models) for 1900–2005, and the CMIP5 high emission scenario (RCP8.5; 22 models) and medium mitigation scenario (RCP4.5; 22 models) for 2006–2098.

31. Allan, R. & Ansell, T. A new globally complete monthly historical gridded mean sea level pressure dataset (HadSLP2): 1850–2004. *J. Clim.* **19**, 5816–5842 (2006).
32. Tokinaga, H. & Xie, S.-P. Wave- and anemometer-based sea surface wind (WASWind) for climate change analysis. *J. Clim.* **24**, 267–285 (2011).
33. Chen, M. Y., Xie, P. P., Janowiak, J. E. & Arkin, P. A. Global land precipitation: a 50-yr monthly analysis based on gauge observations. *J. Hydrometeorol.* **3**, 249–266 (2002).
34. Schneider, U., Fuchs, T., Meyer-Christoffer, A. & Rudolf, B. *Global Precipitation Analysis Products of the GPCC* (Global Precipitation Climatology Centre, 2008); available at ftp://ftp-anon.dwd.de/pub/data/gpcc/PDF/GPCC_intro_products_2008.pdf (2008).
35. Willmott, C. J. & Robeson, S. M. Climatologically aided interpolation (CAI) of terrestrial air temperature. *Int. J. Climatol.* **15**, 221–229 (1995).
36. Hulme, M., Osborn, T. J. & Johns, T. C. Precipitation sensitivity to global warming: comparison of observations with HadCM2 simulations. *Geophys. Res. Lett.* **25**, 3379–3382 (1998).
37. Sen, P. K. Estimates of the regression coefficient based on Kendall's tau. *J. Am. Stat. Assoc.* **63**, 1379–1389 (1968).
38. Kendall, M. G. *Rank Correlation Methods* (Griffin, 1975).